Obrabotka metallov (tekhnologiya, oborudovanie, instrumenty) = Metal Working and Material Science. 2025 vol. 27 no. 2 pp. 103–125
ISSN: 1994-6309 (print) / 2541-819X (online)
DOI: 10.17212/1994-6309-2025-27.2-103-125

NSTU NETI

Obrabotka metallov - Metal Working and Material Science

Journal homepage: http://journals.nstu.ru/obrabotka_metallov

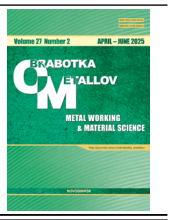

Experimental investigation of graphene oxide-based nano cutting fluid in drilling of aluminum matrix composite reinforced with SiC particles under nano-MQL conditions

Nilesh Patil [1, a], ***Sachin Agarwal*** [2, b], ***Atul Kulkarni*** [3, c, *], ***Atul Saraf*** [4, d], ***Milind Rane*** [3, e], ***Yogiraj Dama*** [5, f]

[1] Maharashtra Institute of Technology, Aurangabad-431010, Maharashtra, India
[2] Deogiri Institute of engineering and management studies, Aurangabad, 431005, India
[3] Vishwakarma Institute of Technology, Pune, Maharashtra, 411037, India
[4] Sardar Vallabhai National Institute of Technology, Surat, 395007, India
[5] Dr. Babasaheb Ambedkar Technological University, Lonere, Raigad, Maharashtra, 402103, India

[a] https://orcid.org/0000-0002-4884-4267, nileshgpatil@rediffmail.com; [b] https://orcid.org/0000-0003-4582-1745, sachinagarwal@dietms.org;
[c] https://orcid.org/0000-0002-6452-6349, atul.kulkarni@vit.edu; [d] https://orcid.org/0000-0003-4776-6874, atul.saraf001@gmail.com;
[e] https://orcid.org/0000-0001-5829-5305, milind.rane@vit.edu; [f] https://orcid.org/0009-0008-5404-4347, yogirajdama@dbatu.ac.in

ARTICLE INFO

Article history:
Received: 12 January 2025
Revised: 12 February 2025
Accepted: 17 March 2025
Available online: 15 June 2025

Keywords:
Nano cutting fluid
NMQL
Graphene oxide
Circularity
Burr height
Empirical modeling

ABSTRACT

Introduction. Minimum Quantity Lubrication (*MQL*) is effectively employed as suitable cooling strategy. However, compared to flood cooling, which is widely used in the industry, *MQL* is characterized by a lower heat dissipation capacity. While thermal shock is reported in flood cooling, the use of *MQL* ensures a smoother chip removal and reduces the risk of thermal stress. **Research methods.** Within the scope of this study, experimental investigations were carried out on drilling of aluminum matrix composite (*MMC*) reinforced with silicon carbide (*Al-SiC MMC*) using *AlCrN PVD*-coated drills (drill diameter 8 mm). *MMC* samples were manufactured with varying volume fractions of *SiC* (10–30%). The aim of the experiments was to study the influence of non-edible vegetable oil with the addition of graphene oxide (used as a cutting fluid) on the drilling process of *AlSiC MMC*. The cutting speed (30–150 m/min), feed rate (0.05–0.25 mm/rev), volume fraction of *SiC* (10–30%), and *MQL* flow rate (60–180 ml/h) were selected as input process parameters. Their response parameters were cutting force, torque, surface roughness, hole circularity, and burr height during high-speed drilling of *MMC*. The undi (Calophyllum inophyllum) oil parameters were determined in accordance with the *ASTM 6751* standard. The surface morphology and elemental analysis of graphene oxide were investigated using scanning electron microscopy (*SEM*) and energy-dispersive X-ray spectroscopy (*EDAX*). **The purpose of the work.** The use of nano-cutting fluid in combination with *MQL* is one of the promising approaches for further improving the characteristics of *MQL*, especially when drilling difficult-to-machine materials. The introduction of nanomaterials into *MQL* contributes to reducing friction at the tool-chip interface, which leads to a decrease in cutting temperature. These methods facilitate the machining of lightweight and difficult-to-machine materials, in particular, aluminum-based metal matrix composites (*MMCs*), which are widely used in the automotive and aerospace industries. **Results and Discussion.** It was found that the use of graphene oxide nanoparticles dispersed in non-edible undi (Calophyllum inophyllum) oil represents a promising alternative to traditional cutting fluids in drilling *MMC*. The aim of the study was to develop semi-empirical models for predicting surface roughness and temperature for various compositions of *MMC*. Increased cutting efficiency is achieved by precisely determining the temperature in the machining zone. However, the practical determination of the cutting temperature in each specific case involves significant labor and financial costs. It was additionally found that graphene oxide nanoparticles mixed with non-edible undi (Calophyllum inophyllum) oil represent an effective alternative to traditional cutting fluids in drilling *MMCs*. The present work develops a comprehensive empirical formula for predicting the theoretical temperature and surface roughness. It was found that the majority of the power input into the machining process is transformed into thermal energy.

For citation: Patil N., Agarwal S., Kulkarni A.P., Saraf A., Rane M., Dama Y.B. Experimental investigation of graphene oxide-based nano cutting fluid in drilling of aluminum matrix composite reinforced with SiC particles under nano-MQL conditions. *Obrabotka metallov (tekhnologiya, oborudovanie, instrumenty) = Metal Working and Material Science*, 2025, vol. 27, no. 2, pp. 103–125. DOI: 10.17212/1994-6309-2025-27.2-103-125. (In Russian).

*** Corresponding author**
Kulkarni Atul P., Professor
Vishwakarma Institute of Technology,
Pune, Maharashtra, 411037, India
Tel.: 91-2026950419, **e-mail:** atul.kulkarni@vit.edu

List of symbols

f	Feed rate (mm/rev)
V_c	Cutting speed (m/min)
Q	Flow Rate (ml/hr)
V_f	*SiC* Volume Fraction (%)
F_x	Thrust force (N)
T	Torque (Nm)
R_a	Surface roughness (μm)
Bh	Bur height (mm)
Cr	Circularity (mm)
RSM	Response surface methodology
CCD	Central composite design

Introduction

The main purpose of cutting fluid is to provide cooling and lubrication effects in the machining zone. A cutting fluid may reduce tool wear, enhance surface finish, and also contribute to evacuating chips from the machining zone, which supports sustainable machining. However, due to ecological concerns and increasing regulations over contamination and pollution, the demand for renewable and eco-friendly cutting fluids is increasing [1-4]. The "term sustainable manufacturing" refers to the creation of products using non-polluting methods and systems, while also preserving energy and natural resources. Such a model must be financially viable, harmless, and healthful for operators [4-5].

In cutting of few difficult-to-cut materials, the heat generation produces other concerns such as thermal cracks and dimensional inaccuracy. Heat dispersal in machines is usually attained by the application of cutting fluids. However, the rising concern has led governments and allied organizations to impose stringent rules and guidelines to oversee the use, recycling, and discarding of cutting fluids. Hence, the industry aims at switching from wet cooling to more economical yet environmentally friendly alternatives. These options include *MQL*, environmentally friendly cutting fluids, nano-cutting fluids, dry cutting, etc. [6-10].

The *MQL* method is an attractive alternative in which a very small quantity of cutting fluid is applied to the machining zone through a nozzle. In *MQL*, cutting fluid is delivered to the machining area drop by drop or as mist. When applied as mist, cutting fluid is atomized by a jet of air, and the mist is directed at the cutting zone. Extensive research has been conducted on *MQL* techniques [11-12]. Many researchers have used vegetable oil along with *MQL* because vegetable oil is a potential source of environmentally favorable cutting fluid due to a combination of biodegradability, renewability, and excellent lubrication performance [13-15].

Recently, non-edible oils used in cutting processes have performed better than traditional machining oils owing to their high lubricity, which creates a strong intermolecular interface on the workpiece. Non-edible oils such as Neem oil, Karanja oil, Jatropha oil, Castor oil, and Cotton seed oil have been researched and found to be good alternatives to conventional oils in terms of functionality [16-19]. For example, Al_2O_3 nanoparticles of 20 nm size were used in soybean oil with a volume fraction of 1.5 % in base oil. Trials show that *NMQL* provides less friction power at tool-chip and tool-workpiece interfaces due to the rolling effect of nanoparticles and superior cooling performance. In addition, nano-fluid *MQL* effectively removes chips and burrs to improve the surface quality of holes and also increases tool life by achieving the lowest tool wear [20-22].

Sodavadia and *Makwana* [23] investigated the application of nano boric acid solid lubricant suspensions in coconut oil during turning of *AISI 304* austenitic stainless steel with a carbide tool. Nano boric acid solid lubricants of 50 nm particle size were suspended in coconut oil, the base lubricant. The variation of average tool flank wear, surface roughness of the machined surface, and cutting tool temperature with cutting speed and feed rate were identified with nano solid lubricant suspensions in coconut oil.

It has been observed from past literature that the use of nanoparticles in machining, especially drilling, proved beneficial due to their significant lubricating and cooling effects. Many researchers have used different nanoparticles with vegetable and conventional cutting fluids; however, no research has yet been reported on using graphene oxide nanoparticles in non-edible vegetable oil like Undi oil [23-25].

Graphene oxide is a recent material produced from synthetic graphite powder. It has excellent mechanical and thermal properties and is used in many fields such as solar cells, touch screens, and biosensors. One of the exceptional properties of graphene oxide is its superior thermal conductivity, which is as high as 5,800 W/m·K, making graphene oxide particles effective heat transfer channels that can be used as cutting fluids in difficult-to-cut materials such as *MMCs* [26, 27].

The purpose of this research is to study nano-cutting fluid with the minimum quantity lubrication (*MQL*) method for automotive and aerospace applications.

In the current study, graphene oxide particles have been dispersed in Undi oil. To investigate the influence of graphene oxide nanoparticles in drilling *MMC* under different cooling conditions, performance was measured in terms of thrust force, torque, surface roughness, circularity, and burr height. The study aims to understand the impact of adding nanomaterials to cutting fluid on the tool-chip interaction surface and on lowering cutting temperature. The focus is on machining lightweight and hard-to-machine materials, such as aluminum-based metal matrix composites (*MMCs*).

CNC machine, *MQL* system, cutting tool, and surface roughness tester facilities available at the Mechanical Engineering Department of VIIT, Pune, Maharashtra, India, were used for the research work.

Investigation Technique

Aluminium metal matrix composites (*AMCs*) are potential materials for different applications due to their superior physical and mechanical properties. Reinforcements in the metallic matrix improve stiffness, specific strength, and wear properties compared to conventional materials. Aluminium *MMCs* are commonly used in aircraft, aerospace, automotive, and various other fields. However, these materials are usually regarded as exceptionally difficult to cut because of the abrasive nature of the reinforcement particulates (Table 1).

Hence, aluminum metal matrix composites reinforced with *SiC* particles have been selected as the workpiece material for this study. Table1 shows the properties of the machined materials used in this experimental investigation. *SEM* micrograph of *Al-SiC MMC* is shown in Fig. 1 at 300× magnification. Fig. 2, *a* and *b* show the *Al-SiC MMC* plate and *PVD*-coated cemented carbide drill bit, respectively.

Table 1

Properties of the machined materials

Workpiece	Properties				
	Thermal coefficient of expansion (K^{-1})	Specific heat, (J/kg·K)	Thermal conductivity, (W/m·K)	Density, (kg/m^3)	Melting point, (K)
Al/SiC_p/10%	20.7	879	156	2.710	828
Al/SiC_p/20%	17.46	837	150	2.765	828
Al/SiC_p/30%	14.58	795	144	2.798	828

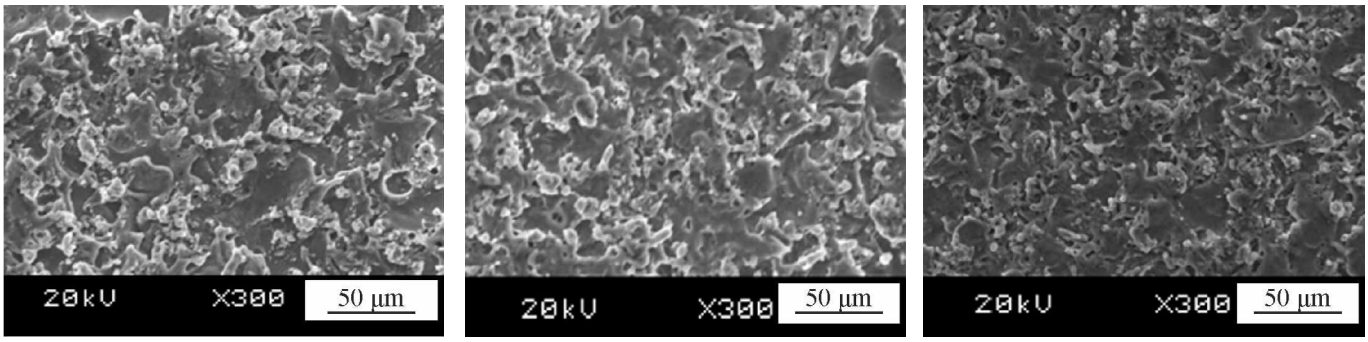

a *b* *c*

Fig. 1. SEM micrographs of *Al/SiC MMC* at *SiC* volume fractions of:
a – 10%; *b* – 20%; *c* – 30%

a *b*

Fig. 2. Al-SiC MMC workpiece material (*a)* and *AlCrN* (*PVD*) coated drill (*b)*

The nomenclature of the *PVD*-coated carbide drill used in this research study was *SD1105A-0680-043-08R1* with a point angle of 140° and 8 mm diameter. This drill was coated with polished *AlCrN* coating. The uniqueness of *AlCrN* coating is that it offers high abrasion resistance, high hardness, good adhesion, and good chip evacuation [27].

A vertical machining center (*BMV 60+* series) was selected for the drilling operation, ensuring highly precise and accurate quality performance with high speed and feed rate. Fig. 3, *a* shows the spike wireless force sensor with tool holder. This wireless force sensor tool holder was used to measure the generated force, torque, and bending moment directly at the tool holder, and the captured data were transmitted to the receiver through a wireless network. The corresponding software processes the data and provides the desired output.

As shown in Fig. 3, *b*, the *MQL* system used in this experiment has two inlet tubes and one discharge pipe that combine in the mixing chamber. One inlet tube was attached to an air compressor, while the other was inserted into a container containing a newly formulated nano-cutting fluid. Based on the air pressure, the oil from the container was pulled out and supplied through the discharge tubes in the form of mist.

For various combinations of process parameters, drilling tests were carried out. The use of Undi oil in metal cutting as a cutting fluid may lead to multiple environmental and agricultural advantages; hence, this oil was selected for experimentation. Undi oil has high survival potential in the environment, remaining stable for up to 50 years. It does not compete with food crops. It serves as a windbreaker at the coast where it can reduce abrasion, protect crops, and offer ecotourism benefits. It has higher oil yield, viscosity, and flash point than generally used non-edible vegetable oils such as Jatropha, Neem, Rubber,

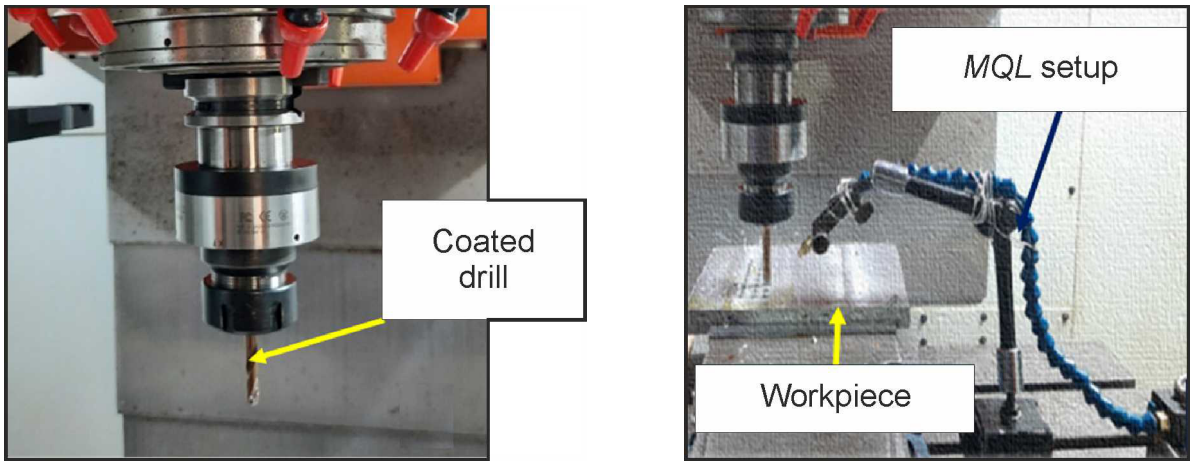

a *b*

Fig. 3. Wireless tool holder (*a*) and *MQL* setup (*b*)

Cotton, Pongamia pinnata, etc. Characterization of Undi oil has been done, and its properties are tabulated in Table 2 as per *ASTM D6751*.

Graphene oxide was used as a nanoparticle to mix with Undi oil to generate the base fluid/coolant. *FESEM* was used to reveal the structure of graphene oxide, as shown in Fig. 4, *a*, which indicates that the size of the graphene oxide sheets is approximately 10 nm. In addition, Fig. 4, *b* shows *EDAX* plots of graphene oxide, which provide evidence of the presence of *C* and *O* ions with the proper ratio, confirming the desired stoichiometric composition. The properties of graphene oxide are given in Table 3.

In order to make nano-cutting fluid, 10 nm-sized graphene oxide nanoparticles were selected due to their potential applications and superior properties. To prepare the nano cutting fluid, four grams of graphene oxide nanoparticles were mixed with 200 ml of Undi oil as the base fluid to prepare the sample. The graphene oxide nanoparticles and Undi oil were mixed in a proportion of 2 w/v % and continuously stirred using a magnetic stirrer for about 24 hours, followed by ultrasonication for 2 hours, as shown in Fig. 5.

Table 2

Properties of Undi Oil

Test Description	Density (g/c^3)	Flash point (°C)	Fire point (°C)	Viscosity (Cst)	Thermal conductivity (W/m K)	Ph range
ASTM 6751	*D1148*	*D93*	*D93*	*D445*	*D2709*	–
Undi Oil	0.91	152	162	38.16	164–168	6.7

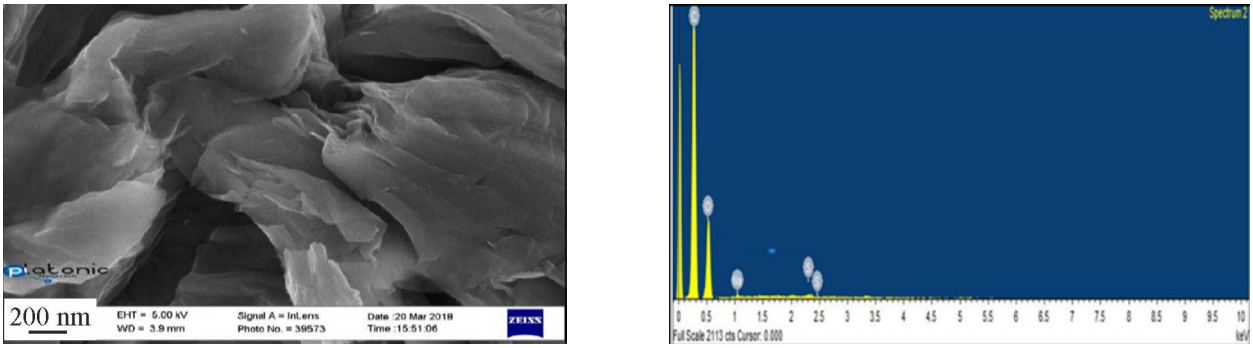

a *b*

Fig. 4. FESEM image of graphene oxide (*a)* and *EDAX* plots of graphene oxide (*b)*

Table 3

Properties of graphene oxide

Specifications	Purity	Thickness	Lateral Dimension	Number of Layer	Surface Area
Values	> 99%	1–5 nm	5–10 μm	Upon the average 4–8	210 m^2/g

Fig. 5. Ultrasonication process for preparation of nano cutting fluid

Response surface methodology (*RSM*) was used for the design of experiments. The objective was to optimize performance measures (responses) influenced by several independent variables commonly known as process parameters. Cutting speed, feed rate, flow rate, and *SiC* volume fraction were selected as process parameters, while thrust force, torque, surface roughness, burr height, and circularity were chosen as responses. Process parameters and their levels were chosen based on literature review and initial trials. Table 4 shows the process parameters and their levels used in the experiments.

Table 4

Machining parameters and levels

Levels	−2	−1	0	+1	+2
Cutting speed (V_c) (m/min)	30	60	90	120	150
Feed rate (f) (mm/rev)	0.05	0.1	0.15	0.2	0.25
Flow rate (Q) (ml/hr)	60	90	120	150	180
SiC vol. fraction (V_f) (%)	10	10	20	30	30

Results and Discussion

A series of trials were carried out on the *VMC* machine using various speeds, feed rates, flow rates, and *SiC* volume fractions. The central composite design (*CCD*) of the response surface method was used for the main experiments, and the corresponding results are tabulated in Table 5. *ANOVA* was used, and the validity of the statistical results was measured with *F*-values and *P*-values. The reliability of the fitted model is recognized by $\boldsymbol{R^2}$. The purpose of the experimental analysis was to determine the significant factors that have the greatest influence on the response variables and to develop a generalized empirical model to

Table 5

Experimental results during *NMQL* condition

Seq. No.	Process Parameters				Responses				
	V_c	f	Q	V_f	F_x	T	R_a	Cr	Bh
	m/min	mm/rev	ml/h	%	N	N·m	μm	mm	mm
1	60	0.1	90	10	282.58	0.783	0.806	0.0287	0.0021
2	120	0.1	90	10	324.21	0.882	0.710	0.0178	0.0436
3	60	0.2	90	10	579.48	1.318	1.784	0.0496	0.0022
4	120	0.2	90	10	577.29	1.282	0.687	0.0300	0.0000
5	60	0.1	150	10	882.81	2.579	2.944	0.0427	0.2926
6	120	0.1	150	10	824.56	2.832	1.326	0.1490	0.3922
7	60	0.2	150	10	1166.5	3.076	2.120	0.0971	0.3675
8	120	0.2	150	10	1059.25	3.114	1.651	0.1385	0.2852
9	60	0.1	90	30	656.62	1.781	2.571	0.1949	0.0800
10	120	0.1	90	30	786.55	1.893	0.075	0.2048	0.1350
11	60	0.2	90	30	1276.03	3.054	0.081	0.1991	0.1827
12	120	0.2	90	30	1206.18	2.688	0.084	0.2059	0.1495
13	60	0.1	150	30	1179.84	3.413	0.089	0.1731	0.2583
14	120	0.1	150	30	1228.36	3.196	0.101	0.1880	0.2706
15	60	0.2	150	30	1534.67	4.604	0.084	0.1873	0.3451
16	120	0.2	150	30	1440.98	3.602	0.224	0.2123	0.3165
17	30	0.15	120	20	953.49	4.131	0.671	0.2559	0.4131
18	150	0.15	120	20	1383.82	4.137	0.921	0.1624	0.332
19	90	0.05	120	20	917.38	3.594	0.208	0.0629	0.5020
20	90	0.25	120	20	1353.33	4.558	0.559	0.1678	0.3343
21	90	0.15	60	20	1186.69	4.363	1.907	0.1621	0.4622
22	90	0.15	180	20	1215.34	4.264	1.505	0.1688	0.4703
23	90	0.15	120	10	1025.96	2.91	2.571	0.1064	0.3380
24	90	0.15	120	30	1389.17	4.215	0.369	0.2225	0.4062
25	90	0.15	120	20	1197.34	4.385	2.122	0.2242	0.4340
26	90	0.15	120	20	1229.32	4.299	1.401	0.1498	0.4634
27	90	0.15	120	20	1253.25	4.406	1.535	0.1522	0.4382
28	90	0.15	120	20	1290.29	4.704	1.578	0.1380	0.5263
29	90	0.15	120	20	1284.21	4.862	1.211	0.0891	0.3630
30	90	0.15	120	20	1275.76	4.881	2.091	0.0817	0.3763
31	90	0.15	120	20	1284.96	4.689	0.921	0.0727	0.4222

predict thrust force, torque, surface roughness, burr height, and circularity. *RSM* explores the relationship between process parameters and responses. Surface plots developed through *RSM* analyze the effect of process parameters on one response while keeping all other process parameters fixed. The relationship between responses and process parameters was visualized by three-dimensional surface plots.

Based on the results, response surface model has been developed for the responses and presented in the equations below.

$$F_x = -3386.81 + 13.4633 \times V_c + 11380.1 \times F + 21.2839 \times Q +$$
$$+114.253 \times V_f - 18.1171 \times V_c \times F - 0.021541 \times V_c \times Q +$$

$$+\ 0.0293687 \times V_c \times V_f - 20.9663 \times F \times V_f - 0.148144 \times Q \times V_f -$$
$$-0.0428178 \times V_c^2 - 18744.4 \times F^2 - 0.0338289 \times Q^2 - 2.17802 \times V_f^2; \quad (1)$$

$$T = -14.04 + 0.057358 \times V_c + 33.1715 \times F + 0.0687884 \times Q +$$
$$0.758479 \times V_f - 0.0672083 \times V_c \times F - 5.11806e - 05 \times V_c \times Q -$$
$$-0.000380625 \times V_c \times V_f - 0.026125 \times F \times Q + 0.243875 \times F \times V_f -$$
$$-0.000403542 \times Q \times V_f - 0.000194778 \times V_c^2 - 75.9202 \times F^2 -$$
$$-0.000144917 \times Q^2 - 0.0164664 \times V_f^2; \quad (2)$$

$$Ra = -1.19377 + -0.00410337 \times V_c + 25.6013 \times F + 0.000873283 \times Q +$$
$$+0.189131 \times V_f + 0.115625 \times V_c \times F + 0.000121597 \times V_c \times Q +$$
$$+0.000195625 \times V_c \times V_f + 0.0477083 \times F \times Q - 0.352375 \times F \times V_f -$$
$$-0.00132646 \times Q \times V_f - 0.000215872 \times V_c^2 - 118.964 \times F^2 +$$
$$+3.69053 \times Q^2 - 0.00138445 \times V_f^2; \quad (3)$$

$$Cr = -0.0466403 - 0.00409958 \times V_c + 1.35925 \times F +$$
$$-0.000901806 \times Q + 0.0216226 \times V_f - 0.002775 \times V_c \times F +$$
$$+1.39861 \cdot 10^{-5} \times V_c \times Q - 1.2625e - 05 \times Q \times V_f +$$
$$+0.00183333 \times 05 \times V_c^2 - 3.23667 \times F^2 + 4.92593e - 06 \times Q^2 -$$
$$-0.000124167 \times V_f^2; \quad (4)$$

$$Bh = -1.59316 + 0.00839594 \times V_c + 2.24223 \times F +$$
$$0.00683264 \times Q + 0.0923996 \times V_f - 0.0147708 \times V_c \times F -$$
$$-4.1875 \times V_c \times Q - 0.000134604 \times Q \times V_f - 3.11267 \times V_c^2 -$$
$$-6.64562 \times F^2 - 5.09895 \times Q^2 - 0.00197624 \times V_f^2. \quad (5)$$

The adequacy of the models has been tested by the correlation coefficient; $\boldsymbol{R^2}$ values in the case of thrust force, torque, surface roughness, burr height, and circularity were found to be 0.9610, 0.9423, 0.9733, 0.957, and 0.964 respectively, which shows good agreement between actual readings and predicted values from the model.

Thrust is the force of reaction against the drill's progress into the workpiece. The test data of the thrust forces as a function of cutting parameters in the drilling of the *Al-SiC MMC* as per *DOE* were observed and recorded. Drilling is a complex process involving a combination of axial (thrust) force and peripheral (torque) force. It has been reported that the most impact on surface deterioration of the workpiece is caused by the thrust force due to the differential flexural characteristics of the matrix and the fiber reinforcement. Thrust force can be used as a process measure to assess the response of the tool-workpiece interface. Any variation in thrust force can be related to a change in the cutting wedge condition, either by deformation, other tool wear modes, or potential interactions between the tool and the heat-affected workpiece in the machining zone [24].

Fig. 6, *a* shows that minimum F_x is observed at 10 % *SiC* volume fraction, while maximum occurs at higher *SiC* volume fractions; similarly, as feed increases, F_x also increases. It has been observed from Fig. 6, *b* that F_x varies according to Q, with maximum F_x at 150 ml/h and 0.2 mm/rev, while minimum at 90 ml/h and 0.1 mm/rev. Fig. 6, *c* shows that maximum F_x is observed at 150 ml/hr and 30 % V_f. It has been observed that as Q increases, F_x also increases; a similar trend has been observed for V_f. However, a rapid increase in F_x occurs as Vf increases from 10 to 20 %, while no significant rise is found after 20 % V_f. Fig. 6, *a* and *b* depict that as f increases from 0.1 to 0.2 mm/rev, F_x also increases rapidly. These results are in agreement with reports by *Gaitonde* et al. [11]. Fig. 6, *a* and *c* indicate that as V_f increases from 10 to 30 %, F_x also increases rapidly; however, no significant difference has been observed between 20 and 30 % V_f – similar findings were reported by *Gaitonde* et al. [12]. It has been seen from Fig. 6, *b* and *c* that minimum F_x is obtained at low Q (90 ml/hr), while maximum is at high Q (150 ml/hr).

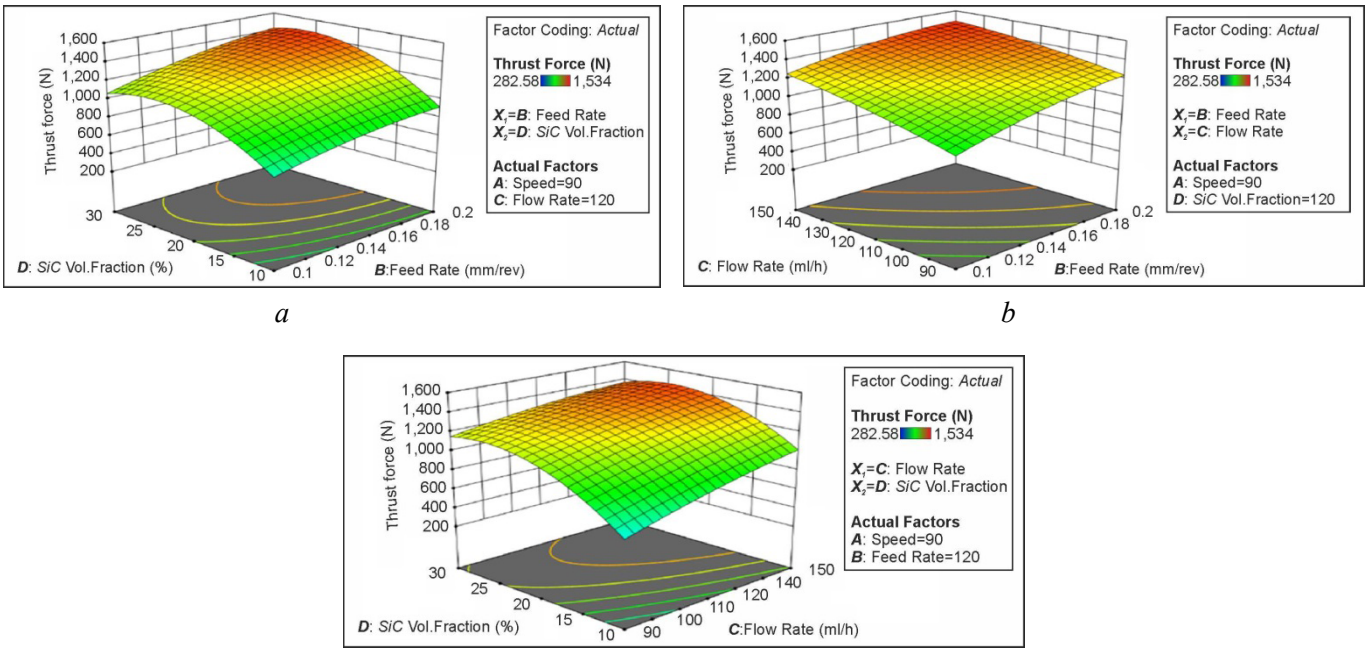

Fig. 6. Effect of cutting speed, feed, *sic* volume fraction and flow rate on thrust force under *NMQL* conditions

Like thrust force, torque also affects the quality of the hole generated. During drilling, the sharp cutting edges over the periphery are often blunt and produce friction by rubbing rather than cutting [18].

The effect of process parameters on torque is shown in Fig. 7. Fig. 7, *a* indicates that as V_f increases from 10 to 30 %, torque also increases rapidly; however, after 20 % V_f, torque shows a slight decrease. It has also been seen that minimum torque occurs at low feed rate and flow rate combination (90 ml/h and 0.1 mm/rev), while maximum occurs at 150 ml/h and 0.2 mm/rev. In addition, Fig. 7, *b* shows that as feed increases from 0.1 to 0.2 mm/rev, torque also increases.

Surface roughness is an indicator of finely spaced micro-irregularities on the surface texture, consisting of three parts: roughness, waviness, and form [24]. It evaluates the surface finish to assess surface irregularities of the workpiece due to machining. It is normally determined as the average roughness (***Ra***), commonly used in the industry. Surface roughness is among the essential aspects of hole quality, where greater surface roughness causes additional wear and fatigue in the material, which directly impacts the production process and cost [21]. It plays a key role in manufacturing and is a major element in assessing machining accuracy [22].

From Fig. 8, *a*, it has been observed that maximum ***Ra*** is seen at 10 % V_f, while it decreases sharply at 30 % V_f. Also, as feed rate increases from 0.1 to 0.2 mm/rev, ***Ra*** increases. Fig. 8, *b* shows that as Q increases from 90 to 150 ml/hr, ***Ra*** also increases sharply. Maximum ***Ra*** is observed at low V_f and high Q (10 % V_f and 150 ml/h), while minimum at high V_f and high Q. Fig. 8, *c* shows maximum ***Ra*** at 10 %

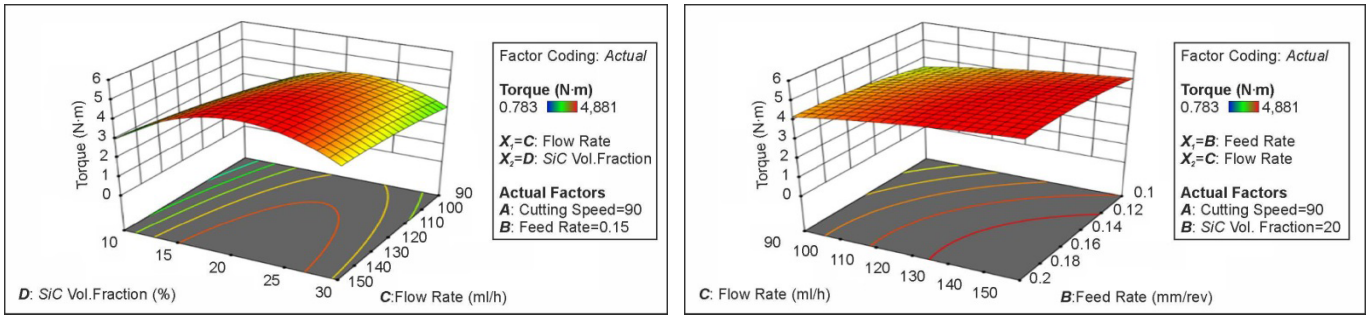

a *b*

Fig. 7. Effect of cutting speed, feed, *SiC* volume fraction and flow rate on torque under *NMQL* conditions

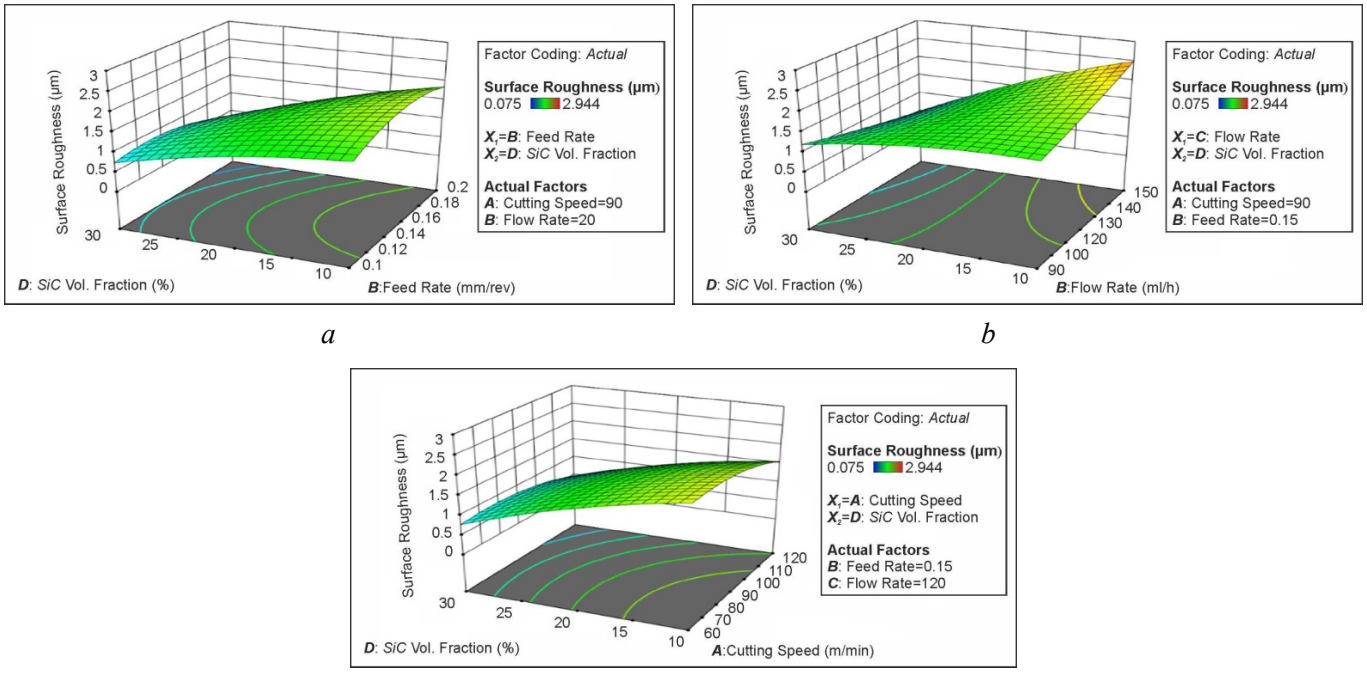

a *b*

c

Fig. 8. Effect of cutting speed, feed rate, *SiC* volume fraction and flow rate on surface roughness under *NMQL* conditions

Vf, while it decreases sharply as V_f increases to 30 %. Also, maximum ***Ra*** is obtained at 60 m/min, while minimum is obtained at 120 m/min.

Fig. 8, *a* shows that as feed rate increases from 0.1 to 0.2 mm/rev, ***Ra*** shows a slightly increasing trend. Lower feed values result in minimum thrust force during drilling, which is one reason for better surface finish at low feed rate [2]. It has been observed from Fig. 8, *b* that ***Ra*** is maximum at 10 % V_f while minimum at 30 % V_f. The increase in V_f decreases ***Ra***, likely caused by increased brittleness and consequent demise of the built-up edge (*BUE*) in machining composite materials (*Gaitonde* et al., 2009). Fig. 8, *b* also shows that as ***Q*** increases from 90 to 150 ml/hr, ***Ra*** also increases, confirming that at low Q, *MQL* can provide better ***Ra*** in drilling. This is possibly due to reduced *BUE* formation from the mist action at the tool-workpiece interface. Fig. 8, *c* shows that as cutting speed changes from 60 m/min to 120 m/min, ***Ra*** decreases. This trend can be explained by the fact that as cutting speed increases, cutting temperature rises, leading to material softening and subsequent reduction in ***Ra***.

Circularity is defined as the degree of roundness of a circular hole. Circularity defines how close a component should be to a perfect circle. Circularity, often called roundness, is a 2-dimensional tolerance that determines the overall shape of a circle and ensures it is not too oval, rectangular, or irregular [2].

It has been observed from Fig. 9, *a* that minimum circularity (***Cr***) is obtained at 0.1 mm/rev and 10 % *SiC* volume fraction, while maximum occurs at 30 % *SiC* volume fraction and 0.2 mm/rev. Fig. 9, *b* shows minimum ***Cr*** at 10 % *SiC* volume fraction and maximum at 30 %, with ***Cr*** increasing with flow rate (minimum at 90 ml/h, maximum at 150 ml/h). Fig. 9, *a* shows minimum ***Cr*** at 0.1 mm/rev and maximum at 0.2 mm/rev; ***Cr*** increases with feed rate, likely due to increased cutting forces. Faster insertion of the drilling tool through the workpiece due to higher feed rate increases hole deformations and vibrations in the cutting tool, resulting in higher circularity errors. Fig. 9, *a* and *b* show ***Cr*** increases rapidly as V_f changes from 10 to 30 %, with minimum ***Cr*** at 10 % and maximum at 30 %.

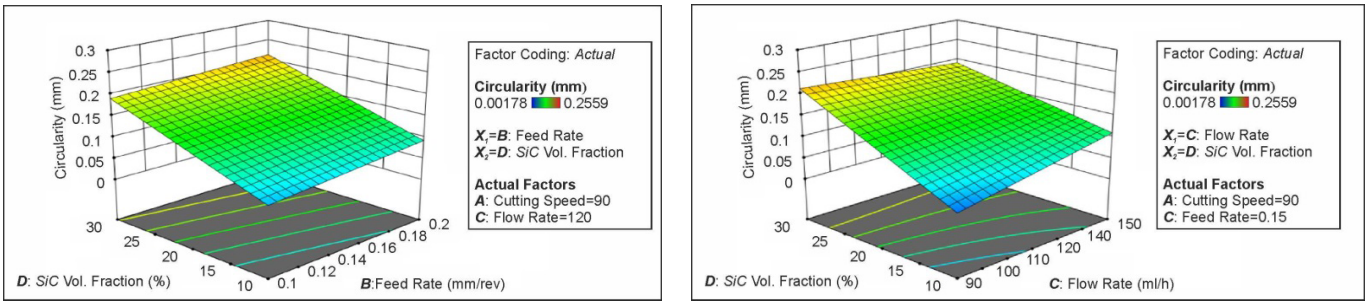

a *b*

Fig. 9. Effect of cutting speed, feed rate, *SiC* volume fraction and flow rate on circularity under *NMQL* condition

Burr is plastically deformed material produced on the edge of the component during drilling. Burrs form and spread circumferentially as the drill feeds into the workpiece. The size of the exit burr is a performance measure of the drilling process that determines the quality of the finished product. It is essential to minimize burr formation at manufacturing stage by choosing proper drilling process parameters.

Fig. 10, *a* shows that as *SiC* volume fraction increases from 10 to 20 %, burr height (***Bh***) increases; however, after 20 % it decreases. As flow rate increases, ***Bh*** increases. Maximum ***Bh*** is obtained at 20 % V_f and 150 ml/h, while minimum at 10 % V_f and 90 ml/h. Fig. 10, *b* shows no significant effect of cutting speed and feed on ***Bh***, although maximum burr height is observed at low feed and cutting speed (60 m/min and 0.1 mm/rev). Fig. 10, *a* shows ***Bh*** increases with ***Q*** from 90 to 150 ml/h due to excessive fluid and nanoparticles at the workpiece-tool and chip-tool interface, which increases cutting force and ploughing during drilling, thus increasing burr height [21]. ***Bh*** increases as V_f changes from 10 to 20 %, but decreases from 20 to 30 %. Fig. 10, *b* shows no significant effect of cutting speed on ***Bh***, although a slight increase at 60 m/min is observed.

Comparison of *MQL* and *NMQL* conditions at different cutting speeds and *SiC* volume fractions was conducted to understand the effect of graphene oxide nanoparticles mixed with Undi oil. Fig. 11 shows that at 10 % *SiC* volume fraction, *MQL* gives better results compared to *NMQL*, while *NMQL* performs equally or better at 20 and 30 % *SiC* volume fractions. This is because graphene oxide nanoparticles have

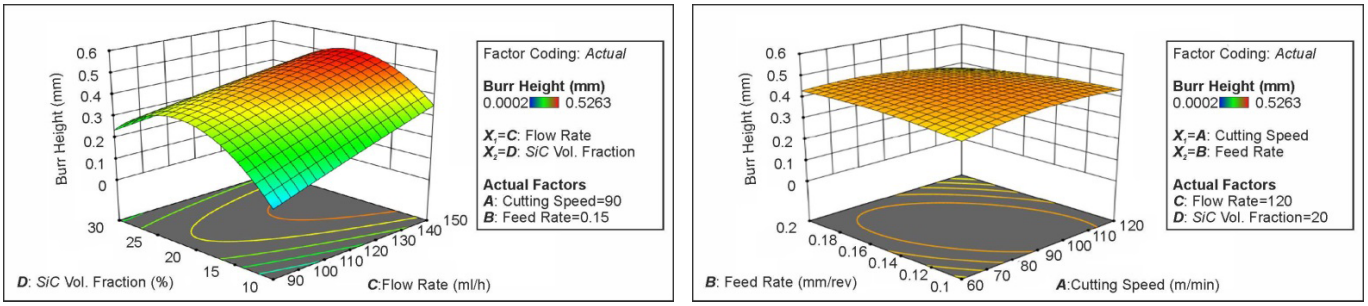

a *b*

Fig. 10. Effect of cutting speed, feed rate, *SiC* volume fraction and flow rate on burr height under *NMQL* condition

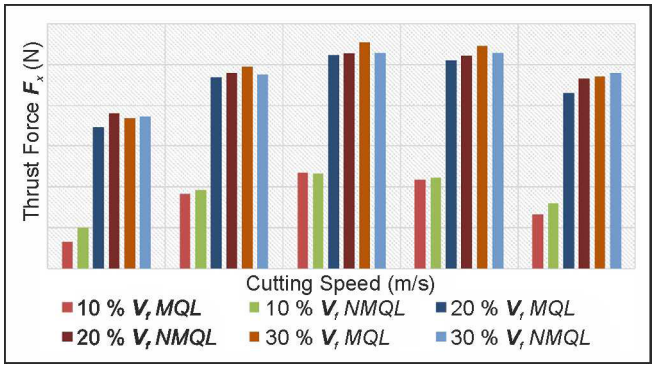

Fig. 11. Comparison of variation of thrust force (F_x) with cutting speed (V_c) and *SiC* volume fraction in drilling

exceptional thermal conductivity and high lubrication capacity. Graphene oxide nanoparticles mixed with Undi oil as an additive can significantly increase thermal conductivity and lubrication, leading to reduced cutting forces. *NMQL* significantly reduces thrust forces compared to *MQL* due to friction reduction at the contact face caused by the rolling effect of nanoparticles and superior cooling performance [16]. Overall, thrust force is minimum at lower *SiC* volume fraction (10 %) and maximum at higher volume fraction (30 %).

Fig. 12 shows that at 10 % *SiC* volume fraction, both *MQL* and *NMQL* give similar torque results. At 20 % *SiC*, *MQL* gives lower torque values. At 30 % *SiC*, *NMQL* performs better; this torque reduction may be due to enhanced lubricity from sliding graphene oxide particles in the cutting fluid [17]. Maximum torque values are obtained at intermediate cutting speeds. Torque reduction is attributed to improved lubrication and cooling by the nanofluid. Lower torque during *NMQL* drilling is due to enhanced thermal conductivity and heat transfer coefficient [19].

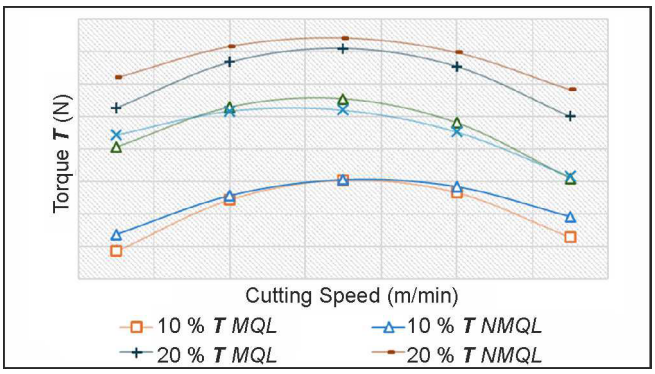

Fig. 12. Comparison of variation of torque (***T***) with feed rate (***f***) and *SiC* volume fraction in drilling

Fig. 13 shows *NMQL* produces less burr height compared to *MQL*. High temperatures generated during *MQL* increase material ductility, producing larger burrs. Overall, burr height is minimum at 10 % V_f and maximum at 20 %. During drilling, heat commonly accumulates at the final machining step due to *BUE* formation as the tool penetrates deeper, affecting exit hole surface quality. *NMQL* minimizes burr formation due to enhanced heat transfer in the cutting zone. *BUE* formation and tool wear are also reduced, leading to less burr [16]. Burr height correlates with thrust force and torque, which decrease greatly under *NMQL*.

Fig. 14 shows that at 30 m/min cutting speed, *MQL* performs better, but at other speeds *NMQL* gives better results for 10, 20, and 30 % *SiC* volume fractions. Under *NMQL*, nanocutting fluid reduces temperature more than *MQL* due to improved thermal conductivity from graphene oxide nanoparticles. Combined lubricating action reduces friction between chip and tool-workpiece interface, aiding smooth sliding. Overall circularity is minimum at 10 % and maximum at 30 % *SiC* volume fraction [20].

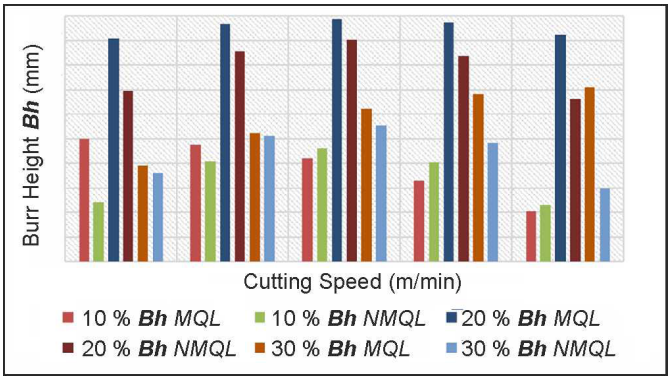

Fig. 13. Comparison of variation of burr height (***Bh***) with feed (***f***) and *SiC* volume fraction in drilling

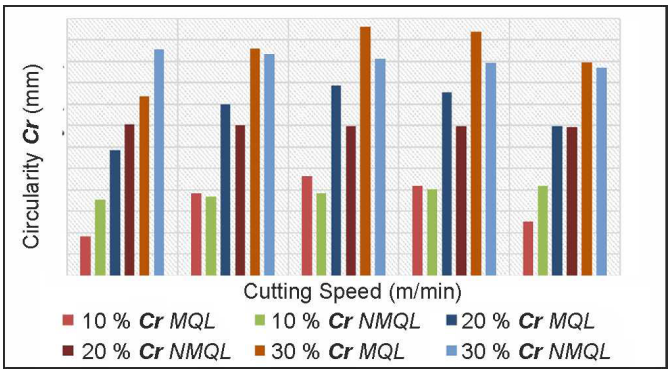

Fig. 14. Comparison of variation of circularity (mm) with cutting speed (V_c) and *SiC* volume fraction in drilling

Fig. 15 shows that at low cutting speeds, *MQL* performs better, while at higher speeds *NMQL* gives better results. At high speeds, lack of heat transfer degrades surface quality due to retained heat. Graphene oxide nanofluids, with higher thermal conductivity, improve heat transfer, reduce friction and temperature, and yield better surface finish. High temperature is eliminated from the machining area due to high thermal conductivity. The ball bearing effect of nanoparticles under *MQL* decreases friction and provides superior cooling and lubrication at the tool-chip interface, reducing tool wear and surface roughness [4].

In this study, the main wear mechanism was abrasion, although adhesion wear was also observed. Different wear types may occur simultaneously or one may dominate due to friction between tool and workpiece. *SEM* results in Fig. 16, *a* show the drill tool micrograph after *NMQL* cooling, and Fig. 16, *b* shows

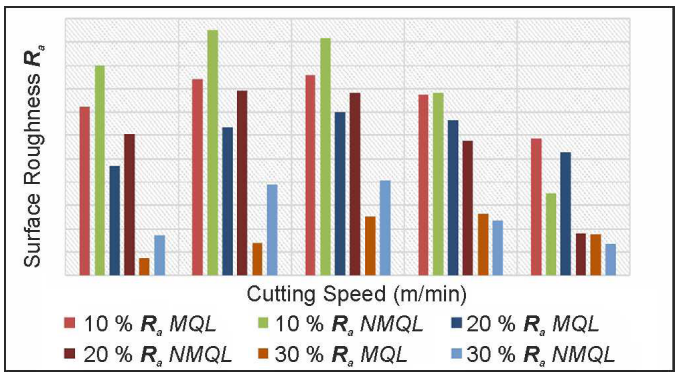

Fig. 15. Comparison of variation of surface roughness (***Ra***) with cutting speed (V_c) and *SiC* volume fraction in drilling

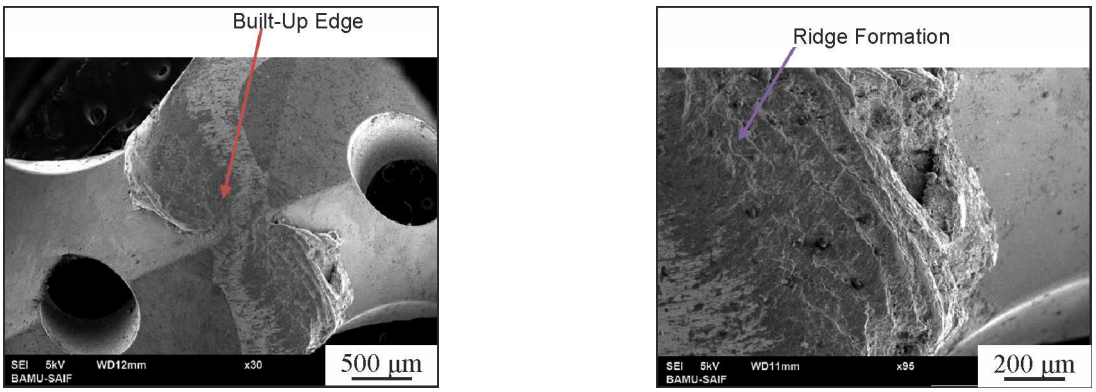

a *b*

Fig. 16. Micrographs of drill tool used in *NMQL* condition after experimentation

an enlarged view. Ridge formation marks are observed on the tool flank face. Due to the high hardness of the tungsten carbide drill tool, abrasion wear in the form of ridges is common for cemented carbide tools. Ridge formation is also caused by the rolling of broken hard carbide tool fragments and nano graphene particles in the cutting zone. During *MMC* drilling, composite particle fragments adhere to the tool forming *BUE*. Coating was worn away from the substrate during drilling due to abrasion and adhesion wear. Built-up edge formation and abrasion marks are clearly visible on the *SEM* micrograph along with prominent ridge formation.

Conclusions

In this experimental investigation, a series of drilling experiments were conducted on *MMCs* with a *PVD*-coated tool to study the effects of nano-graphene oxide suspended cutting fluid on thrust force, torque, surface finish, burr height, and circularity. Based on the study, the following conclusions have been drawn:

1. This investigation confirms that environmentally friendly methods, particularly *NMQL*, can be effectively applied without compromising process results during industrial applications such as drilling *MMCs* with *PVD*-coated carbide drills.

2. Graphene oxide nanoparticles mixed with non-edible Undi oil are a viable alternative to conventional cutting fluids in drilling *MMCs*.

3. *NMQL* provides better hole quality compared to *MQL* due to the combined lubricating action of nanoparticles and Undi oil, which effectively enters interface regions and decreases friction between chip and tool-workpiece interface, resulting in smoother sliding and improved circularity. At high cutting speeds, circularity is maximum; at low speeds, circularity is minimum. Similarly, circularity increases as *SiC* volume fraction increases from 10 to 30 %.

4. Mathematical models describing the relationships between responses and process parameters were developed using *RSM*. Linear regression models best describe these relationships.

5. Burr height increases sharply as *SiC* volume fraction changes from 10 to 20 %, then shows a slight decrease at 30 %.

6. Graphene oxide nanofluids, due to their higher thermal conductivity, improve heat transfer and thus provide better surface finish at high cutting speeds compared to *MQL*.

7. *NMQL* produces less burr height compared to *MQL* because high temperatures during *MQL* increase material ductility, causing greater burr formation.

8. At low cutting speeds, *MQL* yields better surface finish, while at higher cutting speeds, *NMQL* performs better due to higher thermal conductivity reducing friction and temperature.

9. Lower torque values are observed during *NMQL* compared to *MQL*, attributed to better lubricity from graphene oxide particles. Maximum torque occurs at intermediate cutting speeds.

10. Thrust force is maximum at high speeds and minimum at low speeds; similarly, *SiC* volume fraction affects thrust force, with minimum thrust at low volume fractions.

11. Adhesion and abrasion marks with prominent ridge formation are clearly visible on *SEM* micrographs.

12. NMQL produces equal or lower thrust force compared to *MQL* due to the enhanced thermal conductivity and lubrication capability of graphene oxide nanoparticles mixed in Undi oil.

13. Nano cutting fluid with *MQL* techniques improves *MQL* performance, especially in drilling difficult-to-cut materials. Addition of nanomaterials reduces friction at the tool-chip interaction surface, lowering cutting temperature.

14. These techniques are useful in automotive and aerospace applications for machining lightweight, difficult-to-cut materials such as aluminum-based metal matrix composites.

References

1. Aamir M., Giasin K., Tolouei-Rad M., Vafadar A. A review: drilling performance and hole quality of aluminium alloys for aerospace applications. *Journal of Materials Research and Technology*, 2020, vol. 9, pp. 12484–12500. DOI: 10.1016/j.jmrt.2020.09.003.

2. Ali S.H.R. Roles and motivations for roundness instrumentation metrology. *Journal of Control Engineering and Instrumentation*, 2015, vol. 1 (1), pp. 11–28.

3. Amrita M., Srikant R.R., Sitaramaraju A. Performance evaluation of nanographite-based cutting fluid in machining process. *Materials and Manufacturing Processes*, 2014, vol. 29, pp. 600–605. DOI: 10.1080/10426914.2014.893060.

4. Atabani A.E., César A.D.S. Calophyllum inophyllum L. – A prospective non-edible biodiesel feedstock. Study of biodiesel production, properties, fatty acid composition, blending and engine performance. *Renewable and Sustainable Energy Reviews*, 2014, vol. 37, pp. 644–655. DOI: 10.1016/j.rser.2014.05.037.

5. Balandin A.A., Ghosh S., Bao W., Calizo I., Teweldebrhan D., Miao F., Lau C.N. Superior thermal conductivity of single-layer graphene. *Nano Letters*, 2008, vol. 8, pp. 902–907. DOI: 10.1021/nl0731872.

6. Chatha S.S., Pa A., Singh T. Performance evaluation of aluminium 6063 drilling under the influence of nanofluid minimum quantity lubrication. *Journal of Cleaner Production*, 2016, vol. 137, pp. 537–545. DOI: 10.1016/j.jclepro.2016.07.139.

7. Dhar N.R., Islam M.W., Islam S., Mithu M.A.H. The influence of minimum quantity of lubrication (MQL) on cutting temperature, chip and dimensional accuracy in turning AISI-1040 steel. *Journal of Materials Processing Technology*, 2006, vol. 171, pp. 93–99. DOI: 10.1016/j.jmatprotec.2005.06.047.

8. Duc T.M., Long T.T., Van Thanh D. Evaluation of minimum quantity lubrication and minimum quantity cooling lubrication performance in hard drilling of Hardox 500 steel using Al_2O_3 nanofluid. *Advances in Mechanical Engineering*, 2020, vol. 12. DOI: 10.1177/1687814019888404.

9. Fox N.J., Stachowiak G.W. Vegetable oil-based lubricants – a review of oxidation. *Tribology International*, 2007, vol. 40, pp. 1035–1046. DOI: 10.1016/j.triboint.2006.10.001.

10. Fratila D. Environmentally friendly manufacturing processes in the context of transition to sustainable production. *Comprehensive Materials Processing*, 2014, vol. 8, pp. 163–175. DOI: 10.1016/B978-0-08-096532-1.00815-3.

11. Gaitonde V.N., Karnik S.R., Davim J.P. Minimising burr size in drilling: integrating response surface methodology with particle swarm optimization. *Mechatronics and Manufacturing Engineering*. Woodhead Publishing, 2012, pp. 259–292. DOI: 10.1533/9780857095893.259.

12. Gaitonde V.N., Karnik S.R., Davim J.P. Some studies in metal matrix composites machining using response surface methodology. *Journal of Reinforced Plastics and Composites*, 2009, vol. 28, pp. 2445–2457. DOI: 10.1177/0731684408092375.

13. Jomaa W., Mechri O., Lévesque J., Songmene V., Bocher P., Gakwaya A. Finite element simulation and analysis of serrated chip formation during high-speed machining of AA7075–T651 alloy. *Journal of Manufacturing Processes*, 2017, vol. 26, pp. 446–458. DOI: 10.1016/j.jmapro.2017.02.015.

14. Kathirve M., Palanikumar K. Effect of volume fraction on surface roughness in turning of hybrid metal matrix (A6061 A1+SiC+Graphite) composites. *Applied Mechanics and Materials*, 2015, vol. 766–767, pp. 263–268. DOI: 10.4028/www.scientific.net/amm.766-767.263.

15. Katna R., Suhai M., Agrawal N. Nonedible vegetable oil-based cutting fluids for machining processes – a review. *Materials and Manufacturing Processes*, 2020, vol. 35 (1), pp. 1–32. DOI: 10.1080/10426914.2019.1697446.

16. Khanna N., Shah P., Chetan. Comparative analysis of dry, flood, MQL and cryogenic CO_2 techniques during the machining of 15-5-PH SS alloy. *Tribology International*, 2020, vol. 146, p. 106196. DOI: 10.1016/j.triboint.2020.106196.

17. Kishawy H.A., Hosseini A. Environmentally conscious machining. *Machining Difficult-to-Cut Materials*. Springer, 2019, pp. 205–238. DOI: 10.1007/978-3-319-95966-5_7.

18. Ku W.L., Hun C.L., Lee S.M., Chow H.M. Optimization in thermal friction drilling for SUS 304 stainless steel. *International Journal of Advanced Manufacturing Technology*, 2011, vol. 53, pp. 935–944. DOI: 10.1007/s00170-010-2899-5.

19. Lemieux S., Elomari S., Nemes J.A., Skibo M.D. Thermal expansion of isotropic Duralcan meta–matrix composites. *Journal of Materials Science*, 1998, vol. 33, pp. 4381–4387. DOI: 10.1023/A:1004437032224.

20. Vijayaraghavan L. Machining of composites an overview. *International Journal on Design and Manufacturing Technologies*, 2007, vol. 1 (1), pp. 16–23. DOI: 10.18000/ijodam.70004.

21. Manna A., Bhattacharayya B. A study on machinability of Al/SiC-MMC. *Journal of Materials Processing Technology*, 2003, vol. 140 (1–3), pp. 711–716. DOI: 10.1016/S0924-0136(03)00905-1.

22. Sodavadia K.P., Makwana A.H. Experimental investigation on the performance of coconut oil based nano fluid as lubricants during turning of AISI 304 austenitic stainless steel. *International Journal of Advanced Mechanical Engineering*, 2014, vol. 4 (1), pp. 55–60.

23. Muthuvel S., Naresh Babu M., Muthukrishnan N. Copper nanofluids under minimum quantity lubrication during drilling of AISI 4140 steel. *Australian Journal of Mechanical Engineering*, 2020, vol. 18 (suppl. 1), pp. S151–S164. DOI: 10.1080/14484846.2018.1486694.

24. Patil N.G., Brahmankar P.K. Determination of material removal rate in wire electro-discharge machining of metal matrix composites using dimensional analysis. *International Journal of Advanced Manufacturing Technology*, 2010, vol. 51, pp. 599–610. DOI: 10.1007/s00170-010-2633-3.

25. Ralph B., Yuen H.C., Lee W.B. The processing of metal matrix composites – an overview. *Journal of Materials Processing Technology*, 1997, vol. 63 (1–3), pp. 339–353. DOI: 10.1016/S0924-0136(96)02645-3.

26. Ramnath B.V., Elanchezhian C., Annamalai R.M., Aravind S., Sri T., Atreya A., Vignes V., Subramanian C. Aluminium metal matrix composites – a review. *Reviews on Advanced Materials Science*, 2014, vol. 38, pp. 55–60.

27. Kulkarni A., Ambhore N., Deshpande A., Anerao P., Chinchanikar S. Analysis of cutting temperature during turning of SS 304 using uncoated and PVD coated carbide inserts. *Materials Today: Proceedings*, 2022, vol. 68 (6), pp. 2569–2573. DOI: 10.1016/j.matpr.2022.09.417.

28. Dama Y., Jogi B., Pawade R., Kulkarni A. Vliyanie napravleniya pechati na kharakter iznosa PLA-biomateriala, poluchennogo metodom FDM: issledovanie dlya implantata tazobedrennogo sustava [Impact of print orientation on wear behavior in FDM printed PLA Biomaterial: study for hip-joint implant]. *Obrabotka metallov (tekhnologiya, oborudovanie, instrumenty) = Metal Working and Material Science*, 2024, vol. 26, no. 4, pp. 19–40. DOI: 10.17212/1994-6309-2024-26.4-19-40.

29. Pawade R.S., Joshi S.S. Multi-objective optimization of surface roughness and cutting forces in high-speed turning of Inconel 718 using Taguchi grey relational analysis (TGRA). *The International Journal of Advanced Manufacturing Technology*, 2011, vol. 56 (1–4), pp. 57–62. DOI: 10.1007/s00170-011-3183-z.

30. Chinchanikar S. Modelirovanie kharakteristik iznosa pri skol'zhenii kompozitsionnogo materiala na osnove politetraftoretilena (PTFE), armirovannogo uglerodnym voloknom, v pare treniya s SS304 (12Kh18N10T) [Modeling of sliding wear characteristics of Polytetrafluoroethylene (PTFE) composite reinforced with carbon fiber against SS304]. *Obrabotka metallov (tekhnologiya, oborudovanie, instrumenty) = Metal Working and Material Science*, 2022, vol. 24, no. 3, pp. 40–52. DOI: 10.17212/1994-6309-2022-24.3-40-52.

Conflicts of Interest

The authors declare no conflict of interest.